

A simple self-organized swimmer driven by molecular motors

S. GÜNTHER^{1,2} and K. KRUSE^{1,2}

¹ Saarland University, Department of Physics, Campus E2 6, 66123 Saarbrücken, Germany

² Max Planck Institute for the Physics of Complex Systems, Nöthnitzer Str. 38, 01187 Dresden, Germany

PACS 87.16.-b – Subcellular structure and processes
 PACS 47.15.G- – Low-Reynolds-number (creeping) flows
 PACS 05.45.Xt – Synchronization; coupled oscillators

Abstract. - We investigate a self-organized swimmer at low Reynolds numbers. The microscopic swimmer is composed of three spheres that are connected by two identical active linker arms. Each linker arm contains molecular motors and elastic elements and can oscillate spontaneously. We find that such a system immersed in a viscous fluid can self-organize into a state of directed swimming. The swimmer provides a simple system to study important aspects of the swimming of micro-organisms.

Introduction. – Micro-organisms often use flagella or cilia to move autonomously in an aqueous environment [1]. In eukaryotes these hair-like appendages are internally driven by molecular motors. The motors set the appendage into oscillatory motion leading to two- or three-dimensional beating patterns, which propel the organism. Due to the complicated structure of cilia and flagella, our understanding of swimming through these internally driven filaments is still far from being complete. This holds even more for effects caused by hydrodynamic interactions between swimming micro-organisms, which can lead to turbulent motion in bacterial suspensions [2] or to the formation of vortex arrays for ensembles of spermatozoa [3]. In the latter case, the flagella propelling the spermatozoa have been observed to beat synchronously. Synchronous beating can lead to metachronal waves [4] which are of biological importance for the swimming of the single-celled freshwater ciliate paramecium or the transport of mucus in our lungs.

Physical studies of the swimming of micro-organisms have focused on the motion resulting from a given sequence of shape changes. As the Reynolds numbers associated with the flow generated by such swimmers are low, inertial effects do not play a role. Consequently, swimming requires shape changes of more than one degree of freedom [5]. Different swimmer geometries have been considered in this context, see, for example, Refs. [5–10] the simplest being probably the swimmer introduced by Najafi and Golestanian [9,11–13], which consists of three lined-up spheres with periodically varying distances, see Fig. 1a.

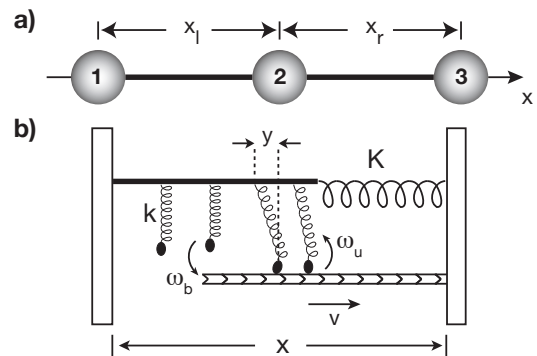


Fig. 1: **a)** Schematic representation of the three-sphere system. **b)** Schematic representation of the dynamic linker element. It consists of a filament, a motor filament, and a linear spring with elastic modulus K . Motors bind to the filament with rate ω_b and unbind with rate ω_u . Motors bound to the filament move with velocity v so as to shorten the linker length x . Motors are connected to the backbone by springs of stiffness k and extension y along the x -axis.

The mechanisms underlying these shape changes, however, have received less attention in the physical community. Exceptions are provided by works on the oscillatory beating of flagella [14–16]. There, the periodic motion is assumed to be generated by spontaneous mechanical oscillations of molecular motors coupled to elastic elements [17, 18]. Combining the action of motor molecules and the bending elasticity of a flagellum, wave

patterns similar to those observed experimentally are generated [14–16].

In this work, we introduce a simple dynamical system consisting of three spheres that are arranged in a line and that are connected by linkers. The linkers consist of molecular motors and elastic elements and their length can oscillate spontaneously. While the swimmer is symmetric with respect to space-inversion the system can dynamically break this symmetry and spontaneously swim directionally. We investigate the system’s bifurcation diagram and provide evidence that the transition to directional swimming shares striking similarities to transitions occurring in integrate-and-fire neurons.

The active three-sphere swimmer. – Consider three spheres, each of radius R moving in a fluid of viscosity η along the x -axis, with neighboring spheres being linked by elements as illustrated in Fig. 1b. Their structure resembles that of sarcomeres, which are the elementary force generating units of skeletal muscle, and consist of motors moving along a polar filament combined with a linear spring. Such structures are known to be able to oscillate spontaneously [18], a phenomenon that has been observed experimentally for muscle sarcomeres [19]. Before investigating the dynamics of the three actively linked spheres, let us first describe the three-sphere swimmer with externally imposed changes of the spheres’ mutual distances.

The three spheres are located at positions x_i , $i = 1, 2, 3$ along the x -axis. At low Reynolds numbers, the forces f_j acting on sphere j with $j = 1, 2, 3$ result in velocities \dot{x}_i according to [20]

$$\dot{x}_i = \sum_j H_{ij} f_j \quad . \quad (1)$$

Here, the mobility tensor H depends on the fluid’s viscosity, the size of the spheres, as well as the distances between them, and satisfies $H_{ij} = H_{ji}$. Using Eq. (1) as well as the global force balance equation $f_1 + f_2 + f_3 = 0$, the velocity of the center of mass of the system, $dx_s/dt \equiv \dot{x}_s = (\dot{x}_1 + \dot{x}_2 + \dot{x}_3)/3$, can be expressed in terms of the distances between the middle and the outer spheres, x_1 and x_r , respectively. For periodically varying distances, one finds for the displacement \bar{x}_s after one period T ,

$$\bar{x}_s = \int_0^T \dot{x}_s dt = \int_O C(x_1, x_r) dx_1 \wedge dx_r \quad , \quad (2)$$

where O denotes the oriented surface encircled in the (x_1, x_r) -plane during one period of the motion, see Fig. 2a and also Refs. [5, 7]. In this expression, C is a field with $C(x_1, x_r) = C(x_r, x_1)$ that only depends on the mobility tensor H . Thus the displacement is independent of the oscillation period. For the calculation of C , it is convenient to employ the Oseen approximation, which consists in expanding H in terms of R/x_1 and R/x_r and retaining leading order terms only. In lowest order, this corresponds

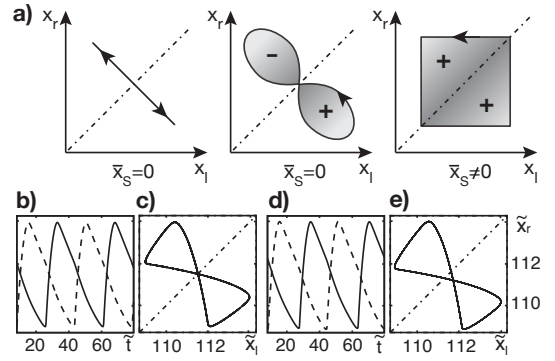


Fig. 2: **a)** Schematic representation of possible orbits in the (x_1, x_r) -plane of periodic motions of the three-sphere system. Left: reciprocal motion, middle: non-reciprocal motion with $\bar{x}_s = 0$, right: non-reciprocal motion with $\bar{x}_s \neq 0$. **b), c)** Left and right linker length as a function of time in the non-swimming state \mathbf{O}_1 , see Fig. 4, with $\xi \gtrsim \xi_s$ and **d), e)** in the swimming state \mathbf{Sw} with $\xi \lesssim \xi_s$. Other parameters as in Fig. 3.

to neglecting hydrodynamic interactions between different spheres. In this case, $C(x_1, x_r) = 0$, implying that hydrodynamic interactions are essential for swimming of the three-sphere system.

If motion is reciprocal, that is, if the corresponding curve in the (x_1, x_r) -plane retraces itself, then $\bar{x}_s = 0$ illustrating Purcell’s Scallop theorem, see Fig. 2a left. Note, that a trajectory which is invariant under the exchange of left and right, i.e., space inversion, is necessarily reciprocal. Examples of other periodic motions with vanishing net displacement are given by $x_1(t) = x_r(t + T/2)$, see Fig. 2a middle. These solutions are invariant under space inversion and a simultaneous shift in time by $T/2$. A simple form of x_1 and x_r with $\bar{x}_s \neq 0$ was proposed by Najafi and Golestanian [9], see Fig. 2a right.

We now describe the dynamics of the linker elements depicted in Fig. 1b, consisting of motors and elastic components. Similar systems have been studied in the contexts of spontaneous spindle [21] and muscle oscillations [22].

A linker element consists of motors moving directionally along a polar filament and a linear spring of stiffness K . The motors are attached to a common backbone by springs of stiffness k and extension y . In a sarcomere, the motors would be ensembles of myosin II that move on an actin filament, while elastic elements are provided by various structural elements, e.g., the protein titin. Motors bound to the filament move such that the linker shortens. An unbound motor binds to the filament at rate ω_b . Attached motors unbind from the filament at rate ω_u . These rates generally depend on the force applied to the motor. We assume that the force dependence is restricted to the unbinding rate. Motivated by Kramers’ rate theory we write $\omega_u = \omega_u^0 \exp\{|f|a/k_B T\}$, where $f = ky$ and a is a microscopic length scale. Also the velocity of bound motors depends on the applied force. For simplicity, we assume a linear force-velocity relation $v(f) = v_0(1 - f/f_0)$. Here, f_0

is the stall force and v_0 the velocity of an unloaded motor.

The dynamic equation for the length x of the linker element connecting two spheres, say 1 and 2, $x = x_2 - x_1$, is given by Eq. (1), where the force f_j on sphere j is the sum of the elastic and the motor forces generated by the linker. The elastic force f_e is given by $f_e = -K(x - L_0)$ with L_0 being the spring's rest length. To calculate the force exerted by the motors, f_m , consider first a single motor bound to the polar filament. If y_n denotes the extension of the spring linking this motor to the backbone then the force it exerts is $-ky_n$. The value of y_n changes according to

$$\dot{y}_n = v_n + \dot{x} \quad , \quad (3)$$

where v_n is the velocity of this motor on the filament. The total motor force then is $f_m = -k \sum_{n=1}^N \sigma_n y_n$. Here, N is the overall number of motors and $\sigma_n = 1$ if motor n is bound and 0 otherwise. We employ a mean-field approximation, which consists in assuming that all bound motors have the same spring extension, $y_n = y$ for all n . We determine the mean position by the product of the average motor speed multiplied with the average time they stay attached, $y = \dot{y}/\omega_u$. For unbound motors, we assume fast relaxation, such that their distribution equals the equilibrium distribution implying $y = 0$ for these motors. Under these conditions, the fraction Q of bound motors evolves according to [21]

$$\dot{Q} = \omega_b - (\omega_b + \omega_u) Q \quad , \quad (4)$$

while the total motor force is

$$f_m = -N(x) Q k y \quad . \quad (5)$$

Here, $N(x) = (\ell_f + \ell_m - x)/\Delta$ is the number of motors in the overlap region of the filament and the motor backbone of lengths ℓ_f and ℓ_m , respectively, and Δ is the distance on the backbone between adjacent motors.

Before considering the active three-sphere swimmer, let us present the dynamics of two actively linked spheres. The dynamic equations for this system are given by Eqs. (1), (3)-(5), where the forces on the spheres 1 and 2 are $f_1 = -f_2 = -f_e - f_m$. To lowest order the Oseen-expansion of H gives $H_{11} = H_{22} = (6\pi\eta R)^{-1}$, and $H_{12} = 0$. H_{ii} is the Stokes friction of an isolated sphere. In dimensionless form, the equations of motion read

$$\xi \dot{\tilde{x}} = -2 \cdot [N(\tilde{x}) Q \kappa \tilde{y} + \tilde{x} - L] \equiv -2 F(\tilde{x}, Q, \tilde{y}) \quad (6)$$

$$\dot{Q} = 1 - [1 + \omega(\tilde{y})] \cdot Q \quad (7)$$

$$\dot{\tilde{x}} = \tilde{y} \cdot [\omega(\tilde{y}) + \gamma] - 1 \quad , \quad (8)$$

where the dimensionless parameters are given by $\xi = 6\pi\eta R \omega_b / K$, $L = L_0 \omega_b / v_0$, $\kappa = k / K$, $\omega = \omega_u / \omega_b$ and $\gamma = kv_0 / (f_0 \omega_b)$. Furthermore, $\tilde{x} = x \omega_b / v_0$ and $\tilde{y} = y \omega_b / v_0$, while time has been rescaled by ω_b .

The equations have a stationary state $(\tilde{x}_0, Q_0, \tilde{y}_0)$. For sufficiently short times, a small perturbation $\delta\tilde{x}, \delta Q, \delta\tilde{y}$ will evolve as $\delta\tilde{x}(t) \propto \exp(st)$ and analogously for δQ

and $\delta\tilde{y}$. It grows if $\Re(s) > 0$. This condition can be expressed in terms of the system parameters¹ and implies $y_0 \omega'_u(y_0) > \omega_b + \omega_u(y_0)$. The force dependence of the binding kinetics is thus essential for an instability of the stationary state. The system oscillates if $\Im(s) \neq 0$ at the instability. This implies $Q_0 k y_0 < K \Delta$, that is, the increase of the motor force by adding one motor in the overlap region needs to be smaller than the corresponding increase of the restoring force by the elastic element to produce an oscillatory instability.

The oscillation mechanism can be understood intuitively as follows: As the motors shorten the linker, the elastic restoring forces increases and, therefore, the force on the motors. This in turn increases the unbinding rate of motors. When a few motors detach from the filament, the remaining motors experience an even higher force, such that an avalanche of motor unbinding events occurs. The elastic element then stretches the linker and the motors rebind, repeating the cycle.

This behaviour shares similarities with the dynamics of integrate-and-fire model neurons [23]. There, the electric membrane potential of a neuron increases monotonically as a consequence of an input current. Upon reaching a threshold value, the potential is instantaneously reset and the loading process restarts. In the case of the linker element, the mechanical analog of neuron's electric potential is the internal stress of the linker. Loading occurs through the action of motors and resetting is accomplished by the spring K after a detachment avalanche of the motors.

Let us now return to the three-sphere system, see Fig. 1, where the spheres are connected by dynamic linker elements. The forces acting on the three spheres are $f_1 = -f_e^l - f_m^l$, $f_2 = -f_1 - f_3$, and $f_3 = f_e^r + f_m^r$, where the superscripts l and r distinguish between the left and the right linker, respectively.

As we have seen above, hydrodynamic interactions between different spheres are essential for swimming of a three-sphere system. Compared to the two-sphere case, we thus now expand the mobility tensor to the next higher order. This leads to $H_{ii} = (6\pi\eta R)^{-1}$, $i = 1, 2, 3$, $H_{12} = (4\pi\eta R)^{-1} R / x_1$, $H_{23} = (4\pi\eta R)^{-1} R / x_r$, and $H_{13} = (4\pi\eta R)^{-1} R / (x_1 + x_r)$. The equations of motion are then given by Eqs. (7) and (8) respectively for the left and right part of the swimmer. Equation (6) is replaced by

$$\xi \dot{\tilde{x}}_{1,r} = \left\{ \frac{3r}{\tilde{x}_{1,r}} - 2 \right\} F(\tilde{x}_{1,r}, Q_{1,r}, \tilde{y}_{1,r}) + \left\{ \frac{3r}{2} \left(\frac{1}{\tilde{x}_1 + \tilde{x}_r} - \frac{1}{\tilde{x}_1} - \frac{1}{\tilde{x}_r} \right) + 1 \right\} F(\tilde{x}_{r,1}, Q_{r,1}, \tilde{y}_{r,1}) \quad (9)$$

with $r = R \omega_b / v_0$. As before, the dynamic equations are invariant under space inversion, i.e., exchange of left and right.

¹The instability occurs at $\xi(1 + \omega(\tilde{y})) + 1 - Q\kappa\tilde{y}\tilde{\Delta} + [N(\tilde{x})Q\kappa(1 + \omega(\tilde{y}) - \tilde{y}\omega'(\tilde{y})) / [\omega(\tilde{y}) + \tilde{y}\omega'(\tilde{y}) + \gamma]] = 0$, with $\tilde{\Delta} = v_0 / \Delta \omega_b$. Here, \tilde{x} , Q and \tilde{y} are taken in the stationary state.

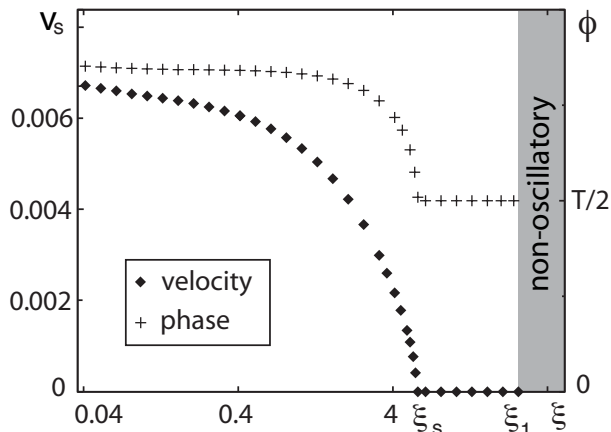


Fig. 3: State diagram of the dynamic three-sphere swimmer. For $\xi > \xi_1$ the system is stationary. Filled diamonds indicate the mean velocity of the swimmer’s center of mass. For $\xi_s < \xi < \xi_1$ it oscillates, but does not move on average, $v_s = 0$. For $\xi < \xi_s$, $v_s > 0$. Crosses indicate the relative phase between the oscillations of the two linker elements. Equations (7)-(9) were solved numerically with $L = 137.5$, $\kappa = 400$, $\omega_0 = 0.5$, $\gamma = 9.1$, $\tilde{\Delta} = 0.16$ and $r = 11$.

Figure 3 summarizes the three-sphere system’s behavior with the active linker elements as the parameter ξ is changed. This can be achieved, for example, by changing the viscosity of the surrounding fluid or the binding rate of the motors. Having $\xi > \xi_1$, the system settles into a stationary state. For $\xi < \xi_1$, the linkers spontaneously oscillate in length. The oscillations of the two linker elements are identical but shifted with respect to each other by half a period. As is illustrated in Fig. 2b,c, this symmetry implies that, for low Reynolds numbers, the swimmer’s center of mass x_s remains stationary on average. There is a second critical value ξ_s , at which the relative phase shift between the two oscillating linkers Φ starts to deviate from half a period, such that the system spontaneously swims if $\xi < \xi_s$. In contrast, the form of the oscillatory motion of each of the two linker elements essentially does not change. By dynamically breaking the space-inversion symmetry, the corresponding orbit in the (x_1, x_r) -plane is not symmetric with respect to the line $x_1 = x_r$, see Fig. 2d,e, hydrodynamic interactions allow in average for directed motion of the three-sphere system.

Decreasing the value of ξ further speeds up the swimmer. The increase in the swimming velocity is the consequence of two effects. On one hand, the relative phase shift gets larger and, on the other hand, the amplitude of the oscillation increases, both leading to larger areas encircled by the orbit in the (x_1, x_r) -plane. For still lower viscosities one expects eventually a decrease in the velocity such that swimming stops at $\xi = 0$. The dynamic equations presented here do not capture this effect as their applicability is restricted to the regime of low Reynolds numbers.

By the symmetry of the swimmer, with each moving state coexists a state moving into the opposite direction.

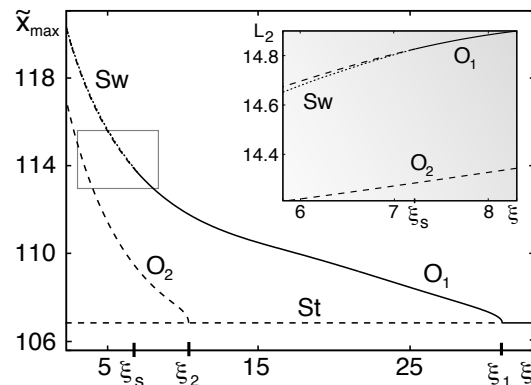


Fig. 4: Bifurcation scenario represented by the linker amplitude \tilde{x}_{\max} for varying parameter ξ . Solid and dotted lines indicate stable, dashed lines unstable states. For $\xi < \xi_1$ the stationary state **St** becomes unstable via a Hopf-bifurcation. The emerging oscillatory state **O₁** loses stability at $\xi = \xi_s$ and the swimming solution **Sw** (dotted line) appears. Furthermore, at $\xi = \xi_2$, a second oscillatory Hopf-mode **O₂** appears. Inset: Representation of the swimming bifurcation in terms of the L_2 -norm (see text).

The actual direction of motion is determined by the initial conditions. Let us also note that changing the parameters γ or r can also lead to transitions from the stationary to the non-swimming oscillatory state or from the non-swimming oscillatory to the swimming state. We did not find two subsequent bifurcations leading from the stationary to the swimming state, though.

We will now take a closer look at the swimming transition. The bifurcation diagram of the swimmer in terms of the oscillation amplitude \tilde{x}_{\max} is presented in Fig. 4. The stationary state **St** loses stability through a supercritical Hopf-bifurcation at $\xi = \xi_1$. The newly generated oscillatory state **O₁** satisfies $\tilde{x}_1(\tilde{t}) = \tilde{x}_r(\tilde{t} + T/2)$, where T is the dimensionless oscillation period. At $\xi = \xi_s$, **O₁** loses stability through a pitchfork bifurcation, see Fig. 3, resulting in the swimming state **Sw**. Here, $\tilde{x}_1(\tilde{t}) = \tilde{x}_r(\tilde{t} + \phi)$, where the relative phase $\phi \neq T/2$. For $\xi < \xi_s$, the states **O₁** and **Sw** have almost the same amplitude. Therefore, we display in the inset of Fig. 4 a representation of the bifurcation in terms of the L_2 -norm, $T^{-1} \int_0^T d\tilde{t} (\tilde{x}_1^2 + \tilde{x}_r^2 + Q_1^2 + Q_r^2 + \tilde{y}_1^2 + \tilde{y}_r^2)$. For a similar value of ξ a second non-swimming state **O₂** bifurcates from the stationary state at $\xi = \xi_2$. This state, which is unstable for all values of ξ , satisfies $\tilde{x}_1(\tilde{t}) = \tilde{x}_r(\tilde{t})$.

The appearance of the state **O₂** together with an inspection of the corresponding isotropy lattice might suggest mode interaction to be at the origin of the symmetry transition. However, the frequencies of **O₁** and **O₂** are different at ξ_s , which argues strongly against mode interaction.

While we are currently lacking a thorough understanding of the swimming transition, we would like to point out that this transition is reminiscent of a phenomenon occur-

ing for two coupled integrate-and-fire neurons [24]. The membrane potential of an integrate-and-fire neuron is increased at a constant rate and reset when a certain threshold voltage is reached. Upon resetting, the neuron sends an electric pulse to other neurons it is connected to and influences their membrane potentials. For broad pulses, the two coupled neurons settle into a state in which they fire periodically with a relative phase shift of half the period. For short enough pulses, however, this state is unstable and a new value of the phase-shift is generated [24]. For the swimmer, in analogy to the electrical pulses for the neurons, mechanical pulses are transmitted between the two linkers. A mechanical pulse is released by one linker when it relaxes as a consequence of a detachment avalanche of the motors. In that case, the duration of the pulse changes, because of alterations of the duration of the linkers expansion phase that effectively transmits the mechanical pulse. Decreasing ξ leads to faster stretching of the linkers. In terms of physical parameters, decreasing ξ either corresponds to reducing friction forces on the beads, to decreasing the binding rate of motors, or to strengthening the elastic elements. As for the two-neuron system, a sharper pulse can be sufficient to cause dephasing [25], which implies swimming.

The equations of motion (7)-(9) are of the form of a singularly perturbed system with ξ as the small parameter. Such systems are known to present strong deformations of a limit cycle close to a Hopf-bifurcation, where the deformation occurs for exponentially small parameter changes [26]. In certain parameter regions, we indeed find that the Hopf-bifurcation is followed by such a deformation which is called a Canard explosion. Accompanying with the Canard phenomenon, we find also excitable dynamics for the swimmer.

In addition to the Canard explosion, the singularly perturbed system (7)-(9) shows dynamic behavior that is reminiscent of the dynamics associated with global bifurcations. In this case, the spontaneous oscillations of the linker are still generated by a Hopf bifurcation. The dynamics close to the bifurcation, however, shows characteristics of the dynamics close to a saddle-node infinite period bifurcation (SNIPER). A SNIPER bifurcation is characterized by two fixed points, a saddle and a node, that collide, which leads to oscillations around a third, unaffected fixed point, namely, an unstable node [27]. In the present case, this limit cycle is symmetric with respect to space-inversion. When decreasing the control parameter ξ further, the limit cycle splits up into two limit cycles that are mirror images of each other upon space inversion. This transition is similar to an anti-gluing bifurcation [28]. A detailed analysis of these bifurcations will be given elsewhere.

Discussion. – In this work, we have presented a simple self-organized swimmer. It consists of three aligned spheres connected by active linker elements that can oscillate spontaneously. By decreasing the dimensionless pa-

rameter ξ below a critical value, which can be achieved either by reducing the the viscosity of the surrounding liquid or the motors' binding rate or by increasing the stiffness K of the elastic element, the system oscillates spontaneously. While this state is not associated with an average displacement, a subsequent bifurcation encountered when decreasing ξ further, leads to directed swimming. Changing other system parameters can either lead to spontaneous oscillations or to swimming but has not been found to induce both transitions subsequently.

Could the self-organized three-sphere be realized experimentally? One approach could be based on muscle sarcomeres as linker elements. As mentioned above, sarcomeres can oscillate spontaneously [19]. Using parameter values appropriate for sarcomeres² and assuming that they link spheres with a diameter of $R = 0.1 \mu\text{m}$, we find swimming velocities on the order of $v_s \approx 1 \mu\text{m}/\text{min}$. This has to be compared to the diffusion constant. For a sphere with a diameter of $0.1 \mu\text{m}$ we find in water at room temperature $D \approx 2 \mu\text{m}^2/\text{s}$. On a distance comparable to the swimmer size $L \approx 3 \mu\text{m}$, diffusion thus dominates the motion $Lv_s/D = 0.025$. In order to reach bigger swimming speeds, the oscillation frequency could be increased. To this end stiffer springs and stronger motors would be necessary. Another way to increase the swimming speed would be through modifications of the swimmer design. For example, it has been argued that the pushmepullyou swimmer [10] is faster than the three-sphere swimmer.

Our self-organized swimmer can be used to study the effects of hydrodynamic coupling between micro-swimmers. So far, studies of this subject have largely neglected the mechanism used by micro-swimmers to generate the shape changes necessary for swimming. Preliminary results suggest interesting synchronization effects that greatly alter the system's behavior compared to swimmers with fixed sequences of shape changes. Obviously, it would also be interesting to extend our approach to study the dynamics of cilia and flagella.

* * *

We thank A. Hilfinger and E. M. Nicola for useful discussions.

REFERENCES

- [1] D. BRAY, *Cell Movements: From Molecules to Motility*, Garland, New York, 2nd edition (2001).
- [2] C. DOMBROWSKI *et al.*, Phys. Rev. Lett. **93**, 098103 (2004).
- [3] I.H. RIEDEL, K. KRUSE, and J. HOWARD, Science **309**, 300 (2005).
- [4] M.A. SLEIGH, in *Cilia and Flagella* edited by M.A. Sleight, (Academic Press, London) 1974, p. 287

² $\ell_f = 0.6 \mu\text{m}$, $\ell_m = 0.75 \mu\text{m}$, $\Delta = 56 \text{ nm}$, $k = 4 \text{ pN/nm}$, $K = 0.01 \text{ pN/nm}$, $L_0 = 1.25 \mu\text{m}$, $v_0 = 2 \mu\text{m/s}$, $f_0 = 4 \text{ pN}$, $k_B T = 4 \text{ pN nm}$, $a = 3 \text{ nm}$, $\omega_b = 220/\text{s}$ and $\omega_u^0 = 120/\text{s}$.

- [5] E.M. PURCELL, Am. J. Phys. **45**, 3 (1977).
- [6] G.I. TAYLOR, Proc. R. Soc. London Ser. A **209**, 447 (1951).
- [7] A. SHAPERRE and F. WILCZEK, Phys. Rev. Lett. **58**, 2051 (1987).
- [8] E.M. PURCELL, Proc. Natl. Acad. Sci. USA **94**, 11307 (1997).
- [9] A. NAJAFI and R. GOLESTANIAN, Phys. Rev. E **69**, 062901 (2004).
- [10] J.E. AVRON, O. KENNETH, and D.H. OAKNIN, New J. Phys. **7**, 234 (2005).
- [11] R. GOLESTANIAN and A. AJDARI, Phys. Rev. E **77**, 036308 (2008)
- [12] R. GOLESTANIAN, Eur. Phys. J. E **25**, 1 (2008)
- [13] R. GOLESTANIAN and A. AJDARI, Phys. Rev. Lett. **100**, 038101 (2008)
- [14] S. CAMALET, F. JÜLICHER, and J. PROST, Phys. Rev. Lett. **82**, 1590 (1999).
- [15] I.H. RIEDEL-KRUSE, A. HILFINGER, J. HOWARD, and F. JÜLICHER, HFSP Journal **3**, 192 (2007)
- [16] S. CAMALET and F. JÜLICHER, New J. Phys. **2**, 24 (2000).
- [17] C.J. BROKAW, Proc. Natl. Acad. Sci. USA **72**, 3102 (1975).
- [18] F. JÜLICHER and J. PROST, Phys. Rev. Lett. **78**, 4510 (1997).
- [19] N. OKAMURA and S. ISHIWATA, J. Muscle Res. Cell Motil. **9**, 111 (1988).
- [20] G.K. BATCHELOR, J. Fluid. Mech. **79**, 1 (1976).
- [21] S. GRILL, K. KRUSE, and F. JÜLICHER, Phys. Rev. Lett. **94**, 108104 (2005).
- [22] S. GÜNTHER and K. KRUSE, New J. Phys. **9**, 417 (2007).
- [23] L. LAPICQUE, J. Physiol. Pathol. Gen. **9**, 620 (1907)
- [24] C. VAN VREESWIJK, L.F. ABBOTT, and G.B. ERMENTROUT, J. Comput. Neurosci. **1**, 313 (1994)
- [25] M. TIMME, private communication.
- [26] E. BENOIT, J.L. CALLOT, F. DIENER, and M. DIENER, Collect. Math. **32**, 37 (1981)
- [27] S.H. STROGATZ, *Nonlinear Dynamics and Chaos*, Addison-Wesley, (1994)
- [28] P. COULLET, J.M. GAMBAUDO, and C. TRESSER, CR Acad. Sci. I-Math. **299**, 253 (1984)